Available online at www.sciencedirect.com
SCIENCE DIRECT
Tectonophysics 415 (2006) 103–121
TECTONOPHYSICS
www.elsevier.com/locate/tecto

Stratigraphic architecture of sedimentary basin induced by mantle diapiric upwelling and eustatic event

Yoshiki Yamada, Masao Nakada *

Department of Earth and Planetary Sciences, Faculty of Science, Kyushu University, Fukuoka, 812-8581, Japan

Received 22 February 2005; received in revised form 17 October 2005; accepted 21 December 2005
Available online 28 February 2006

Abstract

The stratigraphic architecture of sedimentary basin provides important constraints on the rheological structure of the upper mantle and the crust, eustatic events and tectonic movements. In this study, we examined the convective coupling between the uppermost mantle and ductile lower crust as a formation mechanism of sedimentary basins. In this mechanism, the lower crust is squeezed by the upper mantle flow associated with mantle diapiric upwelling, resulting in the surface subsidence and formation of sedimentary basin. We investigated the stratigraphic architecture by taking into account the horizontal migration of the upwelling in time and spatial domains. The sedimentary basin is characterized by both the thickness and formation period for its gross feature and the sequence stratigraphy. The decay of the upwelling causes the surface uplift, and some parts of sediments deposited during the surface subsidence are consequently eroded. The subsidence area moves as the activity of upwelling horizontally migrates, resulting in the formation of unconformity for the uplifted and eroded area over the previous upwelling. We also incorporated the effects of third order eustasy, with amplitude of ~100 m and period of ~1 Myr, into convective coupling model. An application of our model to Karatsu-Sasebo coalfield in the Tertiary of the northwest Kyushu, Japan, indicates that the stratigraphic architecture of sedimentary basin including two effects, i.e. convective coupling and eustasy, may provide important information about the viscosity structure of the lower crust and uppermost mantle and spatio-temporal growth and decay histories of the mantle diapiric upwelling.

Keywords: Sedimentary basin; Eustasy; Mantle diapir; Stratigraphic architecture; Viscosity; Lower crust

1. Introduction

Lithospheric thinning and rifting leading to a formation of sedimentary basin depend primarily on the following three factors: (i) horizontal forces due to plate movement (e.g. Cloetingh and Wortel, 1986; Cloetingh and Kooi, 1992), (ii) convective upwelling of the asthenosphere (e.g. Sengor and Burke, 1978; Huismans et al., 2001) and (iii) thermomechanical structure of the lithosphere (e.g. Goetze and Evans, 1979; Ranalli, 1995; Cloetingh and Burov, 1996). It is also recognized that change in mass due to phase changes within the lithosphere may have played an important role in some phases of extensional settings relevant to basin formation (e.g. Podladchikov et al., 1994; Yamasaki and Nakada, 1997; Petrini et al., 2001; Kaus et al., 2005). The driving forces for the passive and active rifting models, i.e. two end members for rifting

* Corresponding author. Tel.: +81 92 642 2515; fax: +81 92 642 2684.
E-mail address: mnakada@geo.kyushu-u.ac.jp (M. Nakada).

0040-1951/$ - see front matter © 2006 Elsevier B.V. All rights reserved.
doi:10.1016/j.tecto.2005.12.006

model, correspond to the forces related to (i) and (ii) stated above, respectively (Sengor and Burke, 1978; Turcotte and Emerman, 1983; Morgan and Baker, 1983). Sengor and Burke (1978) stated that observed evidences for rifting and rifting-related volcanism wholly support the passive rifting model, whereas Huismans et al. (2001) recently indicated the importance of transition from passive to active rifting.

McKenzie (1978) proposed a lithospheric extension and subsequent thermal contraction model. That is, instantaneous uniform (depth-independent) stretching of the continental lithosphere produces crustal thinning and passive upwelling of hot asthenospheric material. Then the cooling of the lithosphere due to thermal conduction causes the formation of sedimentary basin. This model has been widely accepted as a good first-order approximation for extensional basin subsidence, whereas the differential stretching between the crust and mantle lithosphere has been observed in many basins (e.g. Royden and Keen, 1980; see also compilation by Huismans et al., 2001).

The thermomechanical structure of the lithosphere plays an important role on the modelling of rifting and sedimentary basin (e.g. Burov and Poliakov, 2001; Huismans et al., 2001, 2005). These numerical studies indicated that the model results are significantly sensitive to the rheologies of the lower crust and mantle lithosphere. There are a number of studies indicating the ductile lower crust (e.g. Schmeling and Marquart, 1990; Kaufman and Royden, 1994; Cloetingh and Burov, 1996). For example, Cloetingh and Burov (1996) compared the equivalent elastic thickness (EET) estimated for European continental lithosphere with strength profiles based on the extrapolation of rock mechanics data, and indicated the presence of rather weak lower crustal rheologies, i.e. decoupled lithosphere. They also stated that the decoupled lithosphere is supported from the intra-plate seismicity restricted to the upper crust. On the other hand, the thermomechanical structure of the mantle lithosphere is dominantly sensitive to the temperature distribution of the lithosphere (e.g. Goetze and Evans, 1979; Ranalli, 1995). For example, the existence of lithospheric lid significantly depends on the thermo-tectonic age of the lithosphere (Burov and Poliakov, 2001). Thus, the active rifting model with no lithospheric lid may be applicable to a formation of sedimentary basin in the Japanese Islands as discussed below. Here we investigate a formation of sedimentary basin associated with the convective coupling between the mantle and the crust, which may be applicable to the Tertiary sedimentary basin in the Southwest Japan (e.g. Aihara et al., 1987; Nakada et al., 1997; Yanagi and Maeda, 1998) as discussed below.

Conceptual schemes of convective coupling model (Nakada, 1994) are illustrated in Fig. 1. Fig. 1a shows the lithospheric response to mantle upwelling for an earth model with an elastic lithosphere composed of the uppermost mantle and crust. In this case, the crust uplifts and sedimentary basin is not formed, corresponding to the active model as is observed in the East Africa rift (Ebinger et al., 1989). The sedimentary basin is formed for an earth model with ductile lower crust and no lithospheric lid (Fig. 1b) as may be applied in the Japanese Island arc areas. That is, the ductile lower crust is squeezed by the upper mantle flow associated with the convective coupling between the uppermost mantle and ductile lower crust (lower crustal erosion). The degree of convective coupling is roughly divided into two stages. In the first stage, the upper crust subsides and Moho discontinuity moves upward because of a strong mechanical coupling between the mantle and ductile

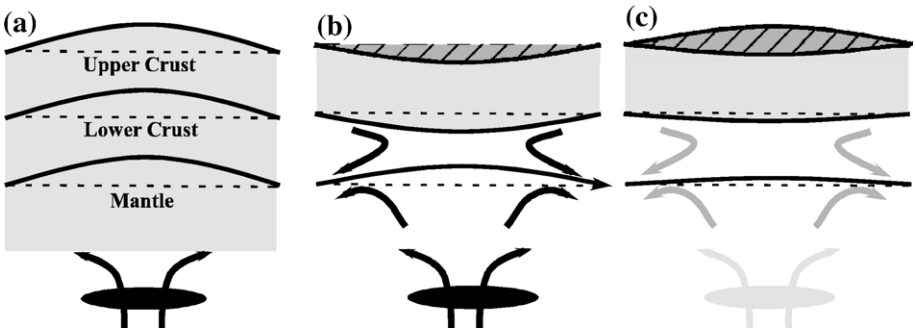

Fig. 1. (a) Schematic crustal and uppermost mantle responses to a mantle diapiric upwelling for an earth model with a lithospheric lid and elastic crust. (b) Schematic illustration showing the responses for an earth model with ductile lower crust and no lithospheric lid. The ductile lower crust is squeezed by the mantle flow associated with the upwelling, resulting in surface subsidence and upward migration of the Moho. (c) In an earth model with ductile lower crust and no lithospheric lid, the lower crust recovers its original thickness as the upwelling decays, resulting in the surface uplift.

lower crust (Fig. 1b), referred to as MC mode by Nakada (1994). Subsequently, the surface keeps subsiding until the force balance between the downward force and flexure of the surface plate (upper crust) is attained, i.e. ~30 Myr after an onset of mantle diapiric upwelling for an earth model with viscosities of $(1–10)\times10^{19}$ Pa s for the lower crust and uppermost mantle. The amount of the subsidence also depends on a scale of the upwelling and flexural rigidity of the upper crust. In the second stage, which has not been discussed by Nakada (1994), the degree of the mechanical coupling is weakened as a decay of upwelling, resulting in the surface uplift (Fig. 1c). The mechanism shown in Fig. 1b and c is, however, effective if the following three conditions are satisfied: (i) ductile lower crust, (ii) mantle diapiric upwelling and (iii) no lithospheric lid below the crust.

The Tertiary sedimentary basins are widely distributed in back-arc region of the Japanese Islands. In the northeastern Japan, the sedimentary basins, probably related to the opening of the Japan Sea, were formed in the back-arc shelf (Sato, 1994). In the northwest Kyushu, Southwest Japan, the Tertiary sedimentary basins were formed followed by the Miocene to Pleistocene basaltic volcanisms (e.g. Yanagi and Maeda, 1998). We assume that the formation of sedimentary basin is tightly related to mantle diapiric upwelling as assumed by Nakada et al. (1997). This long-standing mantle diapiric upwelling beneath northwest Kyushu may be related to an intrinsic upper mantle flow which brings hot mantle material under thicker Asian continental lithosphere towards the boundary as proposed by King and Anderson (1995).

While the fracture strength of the crust increases with increasing depth (Byerlee, 1978), the lower crust is dominated by plastic deformation with increasing temperature (e.g. Goetze and Evans, 1979; Ranalli, 1995; Cloetingh and Burov, 1996). In the spatial distribution of hypocenters of earthquakes in the northwest Kyushu, there are few hypocenters in the lower crust (20–30 km) (Uehira et al., 2001), suggesting ductile lower crust. On the other hand, observed Pn velocity for the land area of the Northeast Japan arc is ~7.5 km s^{-1} and that near the Japan Sea coast is ~8.2 km s^{-1} (Yoshii, 1972; Yoshii and Asano, 1972). The Pn velocity for the land area of Kyushu is ~7.7 km s^{-1} (Fukumitsu et al., 1997) and is also slower than for the Japan Sea coast, suggesting no lithospheric lid beneath the crust of Kyushu area. This may also be supported from the highly conducting layer for the uppermost mantle beneath the northwestern Kyushu and the East China Sea (Shimoizumi et al., 1997), viscosity structure of the uppermost mantle estimated by Holocene sea-level changes for the western part of Kyushu (Nakada et al., 1998) and the observed low-velocity zone in the uppermost mantle beneath the northwest Kyushu (Sadeghi et al., 2000).

The Neogene alkali basaltic volcanism in the back-arc region of the northwest Kyushu, which commenced at ~11 Ma and still continues at present, has been characterized by the type of oceanic island basalts (Nakada and Kamata, 1991; Nakada, 1995; Yanagi and Maeda, 1998). It should be noted that this volcanism is not related to the subduction because the subducted slab has not yet reached under northwestern Kyushu (e.g. Yoshii, 1979, Uehira et al., 2001). In Higashi-Matsuura district with its location of about (33.2°N, 129.8°E) in Fig. 10, upper mantle and ultramafic inclusions are commonly found in an alkali olivine basalt flow (Ishibashi, 1970). The olivine geothermobarometry and clinopyroxene–orthopyroxene thermometry indicate a high temperature of ~1000 °C at 0.8–1.1 GPa (Nakada et al., 1997). Ultramafic xenoliths commonly found in Fukue-jima Island (Fig. 10) also indicate a high geotherm of 1070 °C at 1.0 GPa up to 1200 °C at 2.2 GPa (Umino and Yoshizawa, 1996). That is, these studies indicate a temperature of ~1000 °C at the Moho boundary. Heat flow measurements in this area are very few (only 4 points) and the values are 80 mW m^{-2} around Fukue-jima Island (Uyeda, 1972) and 67–75 mW m^{-2} for the northwestern part of Kyushu (Ehara, 1984; Tanaka et al., 2004). It may be difficult to extract significant information about the temperature around the Moho from these data.

The strength profiles of the lithosphere are estimated using temperatures derived from petrological studies. Shimamoto (1993) estimated the strength profiles based on the rheology of feldspar and feldspathic rocks for the crust and olivine rheology for the upper mantle, and the temperature determined by petrological studies of ~850 °C at the Moho (Tatsumi et al., 1983). The yield stress–depth profile obtained by him indicates ductile lower crust and no lithospheric lid for the Japanese Islands (see also Cloetingh and Burov, 1996). The temperature estimates around the Moho of the northwestern Kyushu indicate that the results by Shimamoto (1993) will be applied to the rheologies of the uppermost mantle and the crust for the northwest Kyushu.

These evidences suggest that the convective coupling mechanism may have effectively operated beneath the northwest Kyushu. Also, there are no evidences that the upper crust has been extended considerably, and the thickness of the crust is ~30 km (Zhao et al., 1992; Uehira et al., 2001). That is, the original McKenzie model cannot be applied to this sedimentary basin,

whereas sedimentary basin can be formed without significant crustal stretching (e.g. Royden and Keen, 1980; Huismans et al., 2001).

Nakada et al. (1997) concluded that the convective coupling mechanism makes it possible to form a sedimentary basin with sediment thickness of ~1000 m for about 30 Myr after an onset of mantle diapiric upwelling as observed in the Tertiary sedimentary basin in the northwest Kyushu. In this study, we incorporate three more plausible processes into the sedimentary basin formation associated with the convective coupling model. The first point is to quantitatively evaluate the effects of growth and decay histories of the upwelling. The mechanical coupling between the mantle and ductile lower crust becomes less effective as the upwelling decays. Then, the lower crust renews its original thickness and the upper crust dragged by the mechanical coupling uplifts. The second point is to incorporate the effects of sedimentation and erosion into crustal movements. Nakada et al. (1997) estimated the total subsidence by only supplying the sediment load into the final subsided area caused by the convective coupling. However, an incorporation of sedimentation related to the crustal movement is required to extract information about the convective upwelling from various geological observations on the structure of sedimentary basin. The third point, essential for applying the numerical results to actual geological observations, is to incorporate the effects of eustatic events (Haq et al., 1987) into the convective coupling model. We therefore adopt a more plausible model and investigate the stratigraphic architecture of sedimentary basin (e.g. Homewood et al., 1999).

In this study, we give a mathematical formulation to describe the stratigraphic architecture, and simulate the stratigraphic architecture including the effects of both the convective coupling and eustatic events. Finally, we apply the results to the Tertiary sedimentary basin in the northwestern Kyushu.

2. Model description

2.1. Governing equation

We employ a quasi two-dimensional incompressible viscoelastic Maxwell body with a multi-layer structure. The earth model used in this study is illustrated in Fig. 2. The upper crust is treated as an elastic layer with a density of 2800 kg m^{-3} and a rigidity of 2.66×10^{10} Pa. That is, the upper crust is assumed to retain flexural strength during a formation of sedimentary basin, which plays an important role on the vertical and horizontal scales as discussed below in detail (e.g. Turcotte and Schubert, 1982; Weissel and Karner, 1989; Nakada, 1994; Watts, 2001). The lower crust is assumed to be Maxwell viscoelastic with a density of 2900 kg m^{-3} and a rigidity of 4.11×10^{10} Pa. The thickness of the crust is assumed to be 30 km, and those for the upper and lower crust are denoted by h_{UC} and h_{LC}, respectively. Here we examine the cases with thicknesses of 10 and 20 km for h_{UC} and h_{LC}. The mantle is treated as a viscoelastic body with a density of 3375 kg m^{-3} and a rigidity of 6.75×10^{10} Pa. The viscosity at an infinite depth is assumed to be 2×10^{20} Pa s as inferred from the Holocene sea-level variations in the post-glacial rebound phase (e.g. Nakada and Lambeck, 1989). The densities ρ (kg m^{-3}) and rigidities μ (Pa) adopted above are similar to those for the Preliminary Reference Earth Model (PREM; Dziewonski and Anderson, 1981). The viscosities of the lower crust (η_{LC}) and uppermost mantle (η_{UM}) for 30–130 km depth are treated as parameters because the predictions are very sensitive to these values.

The governing equation for each layer derived from constitutive and momentum equations is given by

$$\begin{bmatrix} \frac{d\tilde{\hat{u}}}{dz} \\ \frac{d\tilde{\hat{w}}}{dz} \\ \frac{d\tilde{\hat{\sigma}}_{xz}}{dz} \\ \frac{d\tilde{\hat{\sigma}}_{zz}}{dz} \end{bmatrix} = \begin{bmatrix} 0 & k & \frac{1}{\hat{\mu}} & 0 \\ -k & 0 & 0 & 0 \\ 4\hat{\mu}k^2 & \rho g k & 0 & k \\ \rho g k & 0 & -k & 0 \end{bmatrix} \begin{bmatrix} \tilde{\hat{u}} \\ \tilde{\hat{w}} \\ \tilde{\hat{\sigma}}_{xz} \\ \tilde{\hat{\sigma}}_{zz} \end{bmatrix} \quad (1)$$

where u, w, σ_{xz}, and σ_{zz} denote the horizontal and vertical displacements and stress components, respectively (e.g. Cathles, 1975; Wolf, 1985; Nakada, 1994). In Eq. (1), rigidity only appears because the elastic property for an incompressible body is characterized by one elastic parameter (e.g. Cathles, 1975; Wolf, 1985). The circumflex and tilde denote the Laplace transform and Fourier transform, respectively. k (m^{-1}) is wave number and gravity, g, is assumed to be constant. The Laplace transformed rigidity, $\hat{\mu}(s)$, is given by

$$\hat{\mu}(s) = \frac{\mu s}{s + \frac{\mu}{\eta}} \quad (2)$$

where s (s^{-1}) is the Laplace transform variable (Cathles, 1975; Wu and Peltier, 1982). For an adopted earth model, we evaluate the responses to both an internal load (mantle upwelling) and an external load (sedimentation).

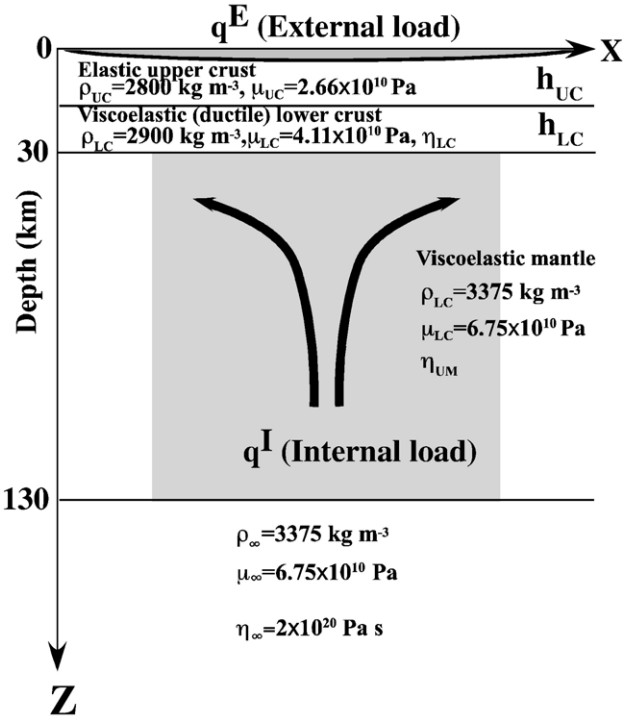

Fig. 2. Model configuration for quasi two-dimensional semi-infinite incompressible Maxwell body adopted in this study. The first, second and third layers correspond to the upper crust, lower crust and uppermost mantle, respectively. The physical parameters in each layer are density (ρ), rigidity (μ) and viscosity (η). The upper crust is assumed to be elastic. The physical parameters except for the viscosity are taken from the Preliminary Reference Earth Model (PREM) by Dziewonski and Anderson (1981). The external load q^{E} (sediment load) is given at the surface, and the internal load q^{I} is assumed to be located in the third layer.

Eq. (1) can be solved by a propagator matrix method (e.g. Cathles, 1975; Nakada, 1994). The solution for the depth z_∞ ($z_\infty > 130$ km), referred to as starting solution here, can be obtained using two parameters, c_1 and c_2, which depend on wave number k and Laplace transform variable s. The starting solution is propagated upwards by considering the continuity of displacement and stress. At the depth of the internal load, we impose the condition of a jump of the normal stress corresponding to the internal load. These procedures make it possible to get the solution at the surface with unknown c_1 and c_2. Furthermore we impose the boundary conditions for σ_{xz} and σ_{zz}, i.e. stress-free condition and normal stress related to external load, and estimate the values for unknown c_1 and c_2. By defining the kernel solutions, K^{I} and K^{E}, for the responses to an internal load, q^{I}, and an external load, q^{E}, the responses are given by

$$\tilde{\hat{Y}}_i = \tilde{\hat{K}}_i^{\mathrm{E}} \cdot \tilde{\hat{q}}_i^{\mathrm{E}} + \tilde{\hat{K}}_i^{\mathrm{I}} \cdot \tilde{\hat{q}}_i^{\mathrm{I}} \tag{3}$$

where $(Y_1, Y_2, Y_3, Y_4)^T = (u, w, \sigma_{xz}, \sigma_{zz})^T$. The external load, q^{E}, is a function of vertical displacement w. That is, Eq. (3) is an integral equation for Y_i.

2.2. Internal and external loads

The thickness (L) and effective width (σ) of the internal load are 100 km and 100 km, respectively, and its density anomaly ($\Delta\rho$) is 10 kg m^{-3}. The density anomaly corresponds to thermal anomaly (ΔT) of ~100 K for a typical thermal expansion coefficient (α) of 3×10^{-5} K^{-1}. The total force for the internal load (F^{I}) is represented by $\Delta\rho L\, g\, e^{-\frac{x^2}{(\sigma/2)^2}}$. Here we assume that the mantle diapiric upwelling, corresponding to the internal load, exists in the uppermost mantle (30–130 km depth). The depth scale of diapiric upwelling is approximately similar to the spatial scale of sedimentary basin examined here (see Fig. 2). As was indicated by Nakada (1994), the contribution of diapiric upwelling below 150 km depth is significantly small, particularly for an earth model with a low viscosity asthenosphere. In this study, we incorporate the following two effects into the internal load model in order to discuss the stratigraphic architecture of sedimentary basin, i.e. (i) growth and decay of the mantle diapiric upwelling and (ii) horizontal migration of the upwelling.

In a modeling of external (sediment) load, we adopt the following assumptions: (i) the subsided area below the sea-level is perfectly filled with sediments and (ii) sediment layer above the sea-level is eroded at a rate, ε, proportional to the uplift (no erosion for $\varepsilon=0$ and perfect erosion for $\varepsilon=1$). The assumption of (i) implying no water load is due to the fact that the basin adopted as a geological application here never presented deep marine conditions as discussed in a later section (Yanagi and Maeda, 1998). However, it should be noted that more realistic loading models involving an interaction between the surface and subsurface processes have been incorporated in recent numerical studies (e.g. Burov and Cloetingh, 1997; Burov and Poliakov, 2001).

The thicknesses related to (i) and (ii) stated above are referred to as $W(t)$ and $H(t)$, respectively. We denote the vertical displacement of the surface at $t=0$

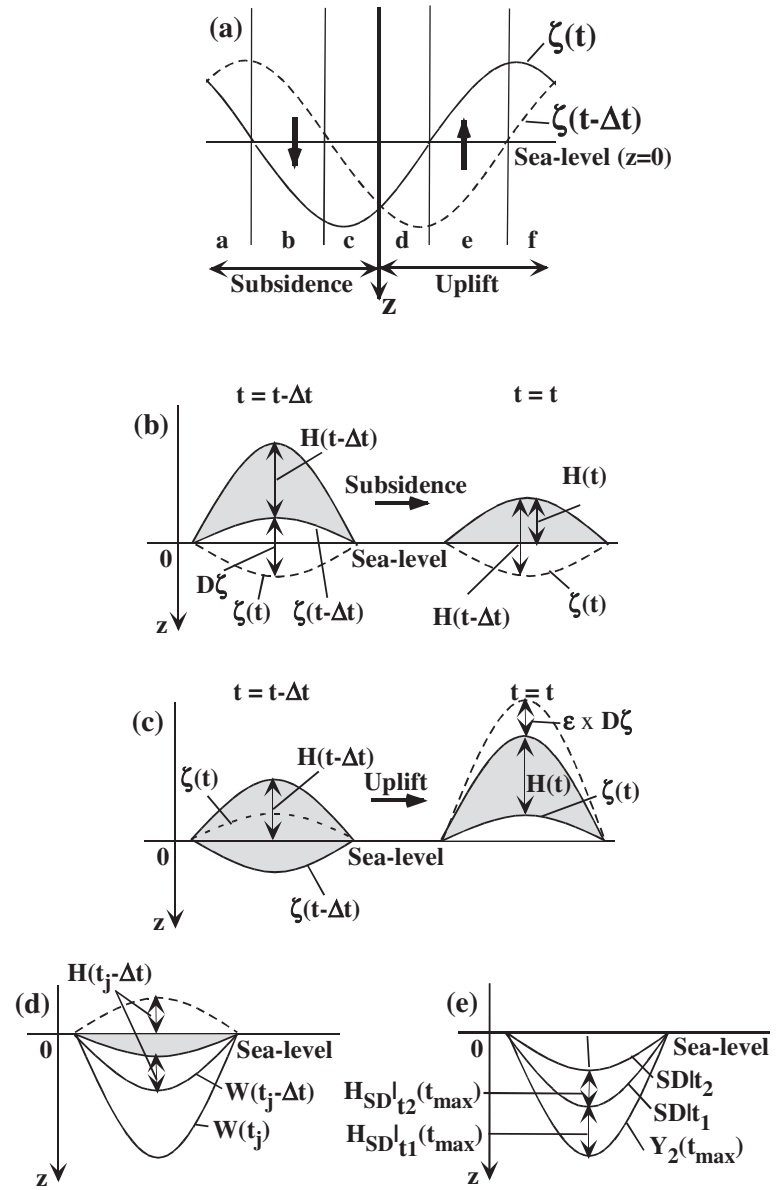

Fig. 3. Schematic illustrations to explain the meanings of Eqs. (4)–(10) in the text. (a) Six cases inferred from the values of $\zeta(t-\Delta t)$ and $D\zeta$ defined by $\zeta(t)-\zeta(t-\Delta t)$. $\zeta(t)$ is the depth of basement. The basement corresponds to the surface at $t=0$, i.e., $\zeta(0)$. (b) For Eq. (5), case (b); (c) for Eq. (6), case (e). (d) A schematic figure for Eq. (9), indicating that the basement has to subside larger than H to deposit sediment additionally. (e) A schematic figure for Eq. (10). Sedimentary layers lap in sequence above the basement, $Y_2(t_{max})$, resulting in a stratigraphic architecture.

(basement) as $\zeta(t)$. Then, we get a form for $W(t)$ as follows:

$$W(t) = \begin{cases} \zeta(t) & (\zeta(t)>0) \\ 0 & (\zeta(t)<0) \end{cases}. \quad (4)$$

The thickness of the sedimentary layer above the sea-level, $H(t)$, is given by using $H(t-\Delta t)$ with $H(0)=0$. Here we define $D\zeta=\zeta(t)-\zeta(t-\Delta t)$. Then we have to investigate six cases for $H(t)$ by taking into account the values of ζ and $D\zeta$ (see Fig. 3a). If the basement subsides ($D\zeta>0$), then we get three cases for $H(t)$:

$$H(t) = \begin{cases} H(t-\Delta t) & (a)\ |D\zeta|<|\zeta(t-\Delta t)|,\ \zeta(t-\Delta t)<0 \\ H(t-\Delta t)-\zeta(t) & (b)\ |D\zeta|>|\zeta(t-\Delta t)|,\ \zeta(t-\Delta t)<0 \\ H(t-\Delta t)-D\zeta & (c)\ \zeta(t-\Delta t)>0 \end{cases}. \quad (5)$$

A schematic figure for the case (b) is illustrated in Fig. 3b. If the value of H is smaller than 0, then we set $H=0$ because of the definition of H. If the basement uplifts ($D\zeta<0$), we get:

$$H(t) = \begin{cases} H(t-\Delta t)+(1-\varepsilon)\cdot|D\zeta| & (d)\ |D\zeta|<|\zeta(t-\Delta t)|,\ \zeta(t-\Delta t)>0 \\ H(t-\Delta t)+\zeta(t-\Delta t)-\varepsilon\cdot D\zeta & (e)\ |D\zeta|>|\zeta(t-\Delta t)|,\ \zeta(t-\Delta t)>0 \\ H(t-\Delta t)-\varepsilon\cdot|D\zeta| & (f)\ \zeta(t-\Delta t)<0 \end{cases}. \quad (6)$$

A schematic figure for the case (e) is shown in Fig. 3c. By adding two parts for the sediment thickness, we get an external load, $q^{\mathrm{E}}(t)$, as follows:

$$q^{\mathrm{E}}(t) = -\rho_{\mathrm{infill}} g[W(t)+H(t)] \quad (7)$$

where ρ_{infill} represents the density of sediment with 2300 kg m^{-3}, and assumed to be constant for simplicity. However, sediment compaction is certainly an important factor for estimating the tectonic subsidence (e.g. Sclater and Christie, 1980) and would change the balance of vertical motions in the basin. Weissel and Karner (1989), for example, examined the effects of sediment compaction in the Rhine graben, and indicated sediment densities ranging in the value of 2260 to 2640 kg m^{-3} as a function of depth. In order to incorporate the effects of compaction into the present model, we have to solve the integral equation allowing for the accommodation space caused by both external and internal loads and the compaction. This is an interesting problem as a future work.

2.3. Sedimentary layer

The Laplace transform inversion for Eq. (3) gives a form for $\tilde{Y}_i(t)$:

$$\tilde{Y}_i(t) = \int_0^t \tilde{K}_i^{\mathrm{E}}(t-\tau)\cdot\tilde{q}^{\mathrm{E}}(\tau)\mathrm{d}\tau + \int_0^t \tilde{K}_i^{\mathrm{I}}(t-\tau)\cdot\tilde{q}_i^{\mathrm{I}}(\tau)\mathrm{d}\tau. \quad (8)$$

The thickness of the sediment which deposits between $t=t_j-\Delta t$ and $t=t_j$, $H_{\mathrm{SD}}|_{t_j}$, is evaluated by taking into account the forms for $W(t)$ and $H(t)$, and given by

$$H_{\mathrm{SD}}|_{t_j} = \begin{cases} W(t_j)-W(t_j-\Delta t)-H(t_j-\Delta t) & \text{for } W(t_j)-W(t_j-\Delta t)-H(t_j-\Delta t)>0 \\ 0 & \text{for } W(t_j)-W(t_j-\Delta t)-H(t_j-\Delta t)<0 \end{cases}. \quad (9)$$

A schematic figure for $H_{\mathrm{SD}}|t_j$ is shown in Fig. 3d. As $H_{\mathrm{SD}}|_{t_j}$ defined by Eq. (9) depends on the crustal movement and erosion after t_j, $H_{\mathrm{SD}}|_{t_j}$ is a function of t ($t>t_j$), i.e. $H_{\mathrm{SD}}|_{t_j}(t)$. In order to describe the stratigraphic architecture of the sedimentary basin, we define the depth of the upper surface of sedimentary layer which deposited from $t=t_j-\Delta t$ and $t=t_j$ as follows:

$$\mathrm{SD}|_{t_j} = Y_2(t_{\max}) - \sum_{n=1}^{j} H_{\mathrm{SD}}|_{t_n}(t_{\max}) \quad (10)$$

where $t_{\max}$ is a final time of computation (see Fig. 3e). A discontinuous plane, referred to as an unconformity here, is formed in the processes of erosion and sedimentation. For instance, we regard $\mathrm{SD}|_{t_q}$ as an unconformity when the thickness of sedimentary layer satisfies the following conditions:

$$H_{\mathrm{SD}}|_{t_p}(t_{\max})\neq 0,\quad H_{\mathrm{SD}}|_{t_q}(t_{\max})=0,$$
$$H_{\mathrm{SD}}|_{t_r}(t_{\max})\neq 0\quad (t_p<t_q<t_r).$$

This condition means that there is a time-related discontinuity between the $H_{\mathrm{SD}}|_{t_p}$ and $H_{\mathrm{SD}}|_{t_r}$.

3. Results

3.1. Characteristics of sedimentary basin for a simple upwelling model

We first examine some characteristics of sedimentary basin based on a simple upwelling model. Table 1 shows viscosity models for examining the effects of viscosity structure of the uppermost mantle (η_{UM}) for 30–130 km depth, lower crust (η_{LC}) and elastic upper crust. In the following discussion, the thicknesses of the upper crust and lower crust are denoted by h_{UC} and h_{LC}, respectively. The internal load adopted here grows up by 1 Myr after an onset of mantle diapiric upwelling. Fig. 4 shows the surface displacement at the load center ($x=0$) for earth models of V1–V5 given in Table 1. We first discuss the results for models V1, V2 and V3 with $\eta_{\mathrm{LC}}=2\times10^{19}$ Pa s and $h_{\mathrm{UC}}=20$ km, in which the viscosity contrasts, $\eta_{\mathrm{UM}}/\eta_{\mathrm{LC}}$, of these models are 1, 10 and 100, respectively (Table 1). Although the subsidence rates for these models are different in the early

Table 1
Viscosity structure models used in this study ($\times 10^{20}$ Pa s)

Model	η (0–10 km)	η (10–20 km)	η (20–30 km)	η (30–130 km)	η (>130 km)
V1	∞	∞	0.2	0.2	2
V1a	∞	0.2	0.2	0.2	2
V2	∞	∞	0.2	2	2
V3	∞	∞	0.2	20	2
V4	∞	∞	2	2	2
V4a	∞	2	2	2	2
V5	∞	∞	20	2	2

stage, those in the later stage are less sensitive to the viscosity of the uppermost mantle. In models V1 and V2, the sedimentary basin is formed mainly in the early stage of 0–30 Myr, but not formed for model V3. The results for models V2, V4 and V5 with $\eta_{UM}=2\times10^{20}$ Pa s and $h_{UC}=20$ km, which have viscosity contrasts, η_{UM}/η_{LC}, of 10, 1, and 0.1 respectively, are also shown in Fig. 4. In a viscosity model of V5 with $\eta_{LC}=2\times10^{21}$ Pa s, the sedimentary basin is not formed in the period of 0–50 Myr. We also illustrate the results including the effects of sedimentation ($\rho_{infill}=2300$ kg m^{-3}) for models V1 and V4, i.e. V1+q^E and V4+q^E in Fig. 4, indicating the importance of sediment loads on the formation of sedimentary basin.

As was discussed by Weissel and Karner (1989), the thickness of an elastic lithosphere plays an important role on the vertical and horizontal scales of the sedimentary basin. In order to discuss this point, we compare the model results for V1 and V4 with those for

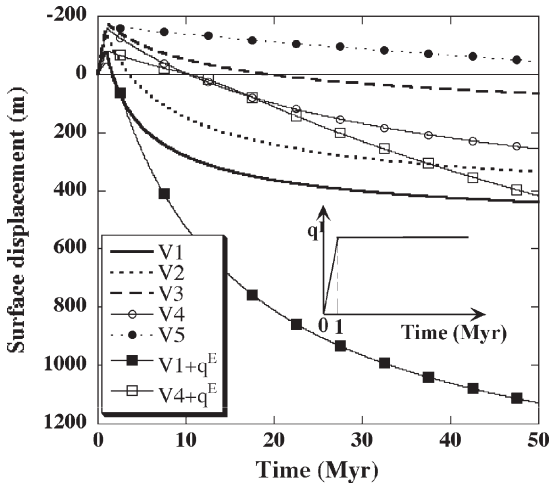

Fig. 4. Time-dependent surface displacement at the center of upwelling for various viscosity structures (see Table 1). The basement corresponds to the surface at $t=0$. The growth period of upwelling is 1 Myr and keeps its strength after reaching its steady state. The results for V1–V5 are for internal load alone, but the results for V1+q^E and V4+q^E include the effects of both internal and external loads.

V1a and V4a. For an internal load model with no sediment load, the surface displacement is determined by the normal stress at the base of the upper crust and the flexural strength of the elastic upper crust. Fig. 5a and b depict the displacement of the surface and Moho discontinuity for models V1, V4, V1a and V4a, respectively, indicating that the responses for V1a and V4a are generally quicker than those for V1 and V4.

Here we examine the results for V1 and V1a at $t=50$ Myr in order to quantitatively discuss the effects of thicknesses of the upper and lower crust. The amounts of the Moho uplift for models V1 and V1a with only internal load are 5260 and 3500 m, respectively, indicating that the lower crustal erosion due to MC mode effectively operates for V1 model with a thinner lower crust. On the other hand, the amounts of surface subsidence for V1 and V1a are 441 and 283 m, respectively. By considering the density of the lower crust, 2900 kg m^{-3}, and the density contrast of 475 kg m^{-3} between the lower crust and mantle, the total subsidence for V1 expected from the migration of the Moho would be 862 m in static (local) isostasy, implying the remaining subsidence of 421 m. In the case of V1a, the total subsidence expected from the Moho uplift is 573 m and the remaining one is 293 m. In both models with no sediment load, therefore, about half of the surface displacement expected from the Moho deformation is supported by the normal stress at the base of the upper crust and flexural strength of the elastic upper crust.

The effects of the thickness of elastic upper crust may be clearly indicated from the results of V1+q^E and V1a+q^E with sediment loads. Fig. 5c and d depict the displacement for the surface and Moho. As was estimated above, the total subsidence expected from the Moho deformation is 1909 m for V1+q^E and 1305 m for V1a+q^E. That is, the amounts of remaining subsidence for V1+q^E and V1a+q^E are 779 and 149 m, respectively, indicating that the mechanical state for V1a+q^E is close to static isostasy. Thus, the flexural strength of elastic upper crust, proportional to h_{UC}^3, plays an important role on the formation of sedimentary basin

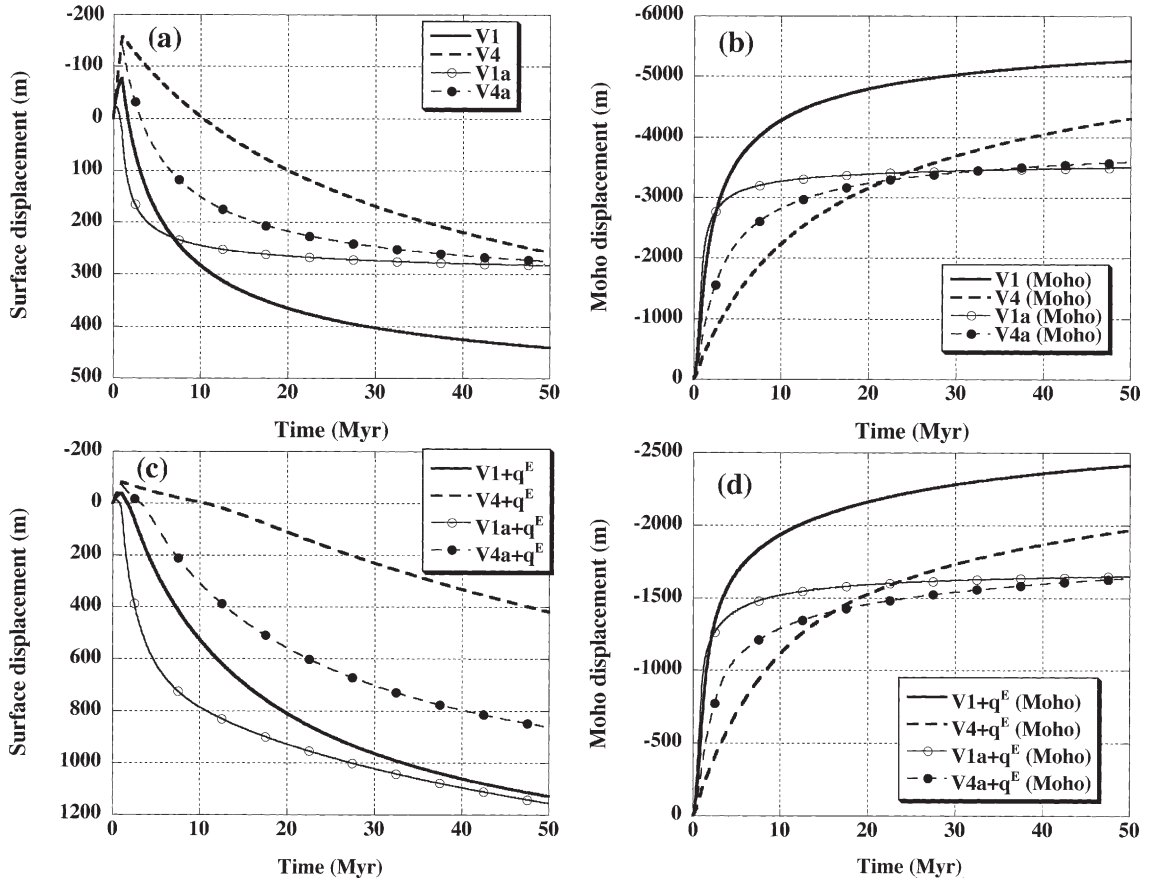

Fig. 5. The displacement of the surface and the Moho at the center of upwelling for viscosity models V1, V4, V1a and V4a (Table 1). The upwelling model is the same as that used in Fig. 4. Model results for (a) and (b) are for internal load alone, but those (c) and (d) include the effects of both internal and external loads.

as well as the thickness of the ductile lower crust. We discuss the effects of these thicknesses on the spatial scale using the results shown in Fig. 8. Model results examined here (Figs. 4 and 5) indicate that the sedimentary basin with a thickness of ~1000 m is formed within 30 Myr after an onset of mantle diapiric upwelling for limited viscosity models with $\eta_{LC} \sim 10^{19}$ Pa s and $\eta_{UM} \sim (1-10) \times 10^{19}$ Pa s. However, the sedimentary basin thicker than 1000 m is not formed within 30 Myr for viscosity models with $\eta_{LC} \geq 10^{21}$ Pa s and/or $\eta_{UM} \geq 10^{21}$ Pa s.

The growth time of the upwelling, γ, plays an important role on the subsidence histories for a convective coupling model adopted in this study. We therefore examine the effects for earth models of V1 and V1a by adopting $\gamma = 1$, 10 and 50 Myr, referred to as GT1, GT2 and GT3, respectively (Fig. 6a). The responses for V1a are quicker than those for V1 as indicated in Fig. 5. The initial uplift of the surface depends on the growth time and the uplift is not predicted as the growth time increases. The surface subsides slowly with increasing growth time, and consequently the amount of the subsidence for model GT3 cannot attain its steady state within 50 Myr. That is, the formation period of this type of sedimentary basin depends on both the viscosity structure and the growth time of mantle diapiric upwelling.

The decay of upwelling causes the surface uplift as stated previously (see Fig. 1c), and the uplift rate strongly depends on the decay rate of upwelling. Fig. 6b depicts the effects of decay rates on the uplift for earth model of V1 and V1a. The decay periods adopted here are 1 Myr, 10 Myr and 50 Myr, referred to as AT1, AT2 and AT3, respectively. In these models, we assume that the growth time is 1 Myr and the decay of the upwelling strength starts at 20 Myr. Rapid responses are predicted for AT1, and the uplift rates decrease with increasing period of the decay.

The erosion rate, ε, also affects the uplift rate significantly. Fig. 6c depicts the effects of erosion rates

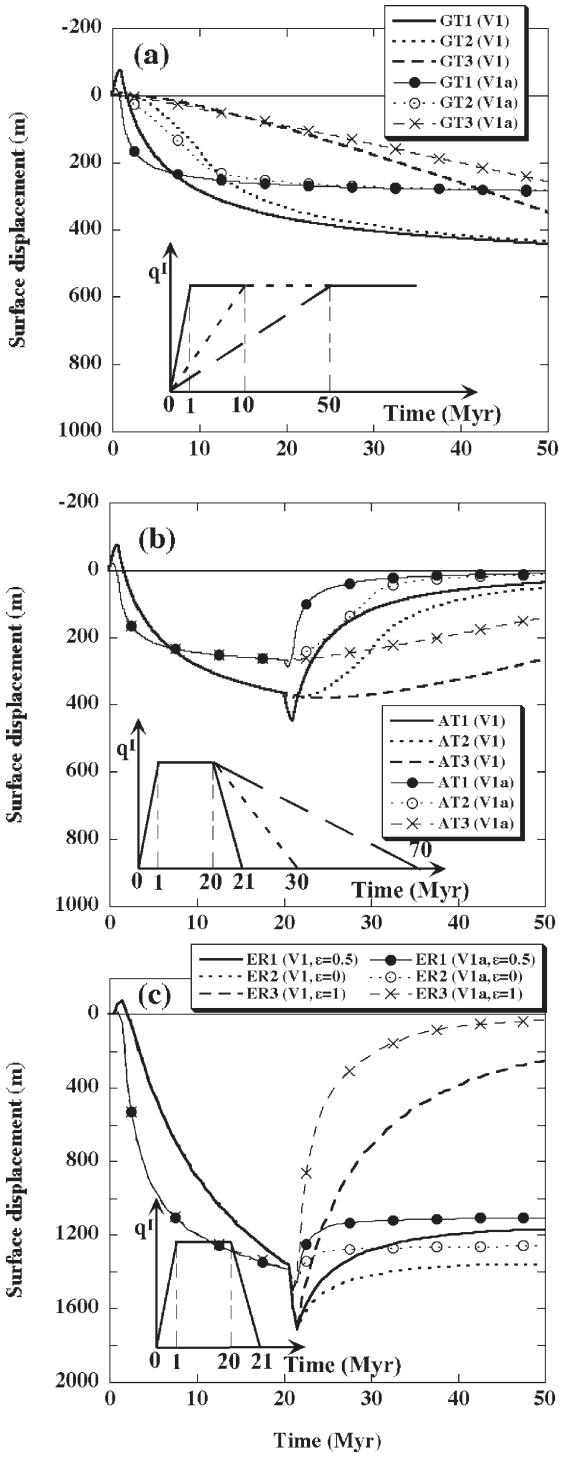

Fig. 6. Time-dependent surface displacement at the center of upwelling for various growth periods of upwelling (a), decay periods of upwelling (b) and erosion rate (c). The viscosity models are V1 and V1a. The results for (a) and (b) include the effects of internal load alone. Adopted upwelling models are shown in each figure.

on the uplift for earth model of V1 and V1a. We examine the effects for AT1 model in Fig. 6b by adopting $\varepsilon = 0.5$, 0 and 1.0, referred to as ER1, ER2 and ER3, respectively. The responses for V1a are also quicker than those for V1. The model with a larger erosion rate, ER3, causes a faster uplift because the uplifted sediment is eroded in sequence, resulting in a thinner sedimentary basin, and vice versa for a smaller erosion rate, ER1. Thus, the uplift rate depends on the viscosity structure, decay rate of the mantle upwelling and erosion rate.

3.2. Pattern of stratigraphic architecture

In the northwest Kyushu, the accommodation space migrated toward northwest (Aihara et al., 1987). This observation may be explained by taking into account the horizontal migration of mantle diapiric upwelling. Here we examine the effects of spatio-temporal changes of the upwelling on stratigraphic architecture of sedimentary basin. The sedimentary basin with a thickness of ~1500 m and formation period within ~30 Myr is mainly investigated because we adopt the Tertiary sedimentary basin of the northwestern Kyushu as a geological application.

We examine two cases for the migration of mantle diapiric upwelling in investigating the horizontal migration of accommodation space. One is the case that the upwelling moves continuously in time domain as shown in Fig. 7a, referred to as UPW1 here. In this case, the migration of accommodation space is caused by a successive event. The other is the case that the upwelling moves discontinuously as shown in Fig. 7b, referred to as UPW2 here. In this case, multiple events cause the migration of accommodation space. We adopt viscosity models of V1 and V1a and erosion rate (ε) with 0.5. The density of sediment filling the subsided area is assumed to be 2300 kg m^{-3}. The growth and decay periods of upwelling are 1 Myr, and other parameters are shown in Fig. 7. The predictions for these two upwelling models are illustrated in Fig. 8, in which the left and right columns represent the results for viscosity models of V1 and V1a, respectively.

We first examine stratigraphic architectures of sedimentary basins for a mantle diapiric upwelling model for UPW1. The width of upwellings is 100 km and the interval of each upwelling is 50 km. Fig. 8a and b illustrate the results at 20 Myr. The gradation color shows the depositional age of sediments. The black lines indicate the depositional age at every 2 Myr and the open circles indicate unconformities. The migration of accommodation space is associated with the horizontal migration of upwelling, and the unconformities are

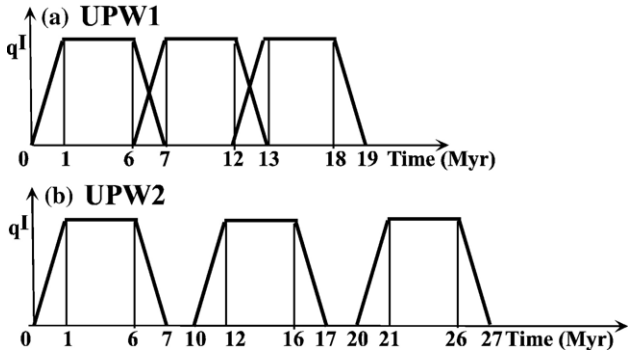

Fig. 7. Time-dependent upwelling models to examine the effects of migration of the activity of upwelling: (a) for continuous migration in time and spatial domains and (b) for discontinuous migration in time domain, i.e. multiple events. These models for (a) and (b) are referred to as UPW1 and UPW2, respectively.

caused by the crustal uplift due to the migration of upwelling. Also, the left side of the sedimentary basin uplifts and the sedimentary layer deposited in the early stage is tilted toward the direction of migration. An unconformity plane covers most of the surface because the surface uplifts when upwelling stops at $t=19$ Myr. Although we recognize some unconformities except for the surface, the sedimentation layer is roughly continuous in chronological order. These features can be seen in both the predictions for viscosity models of V1 and V1a. That is, the accommodation space and the distribution of unconformities are grossly less sensitive to the thicknesses of the elastic upper crust and ductile lower crust. A main difference can be seen for the sediment thickness deposited in the early phase of each upwelling, consistent with the rapid response for viscosity model V1a compared with that for V1 as shown in Figs. 5 and 6. Consequently, the thickness in the early stage is thicker for V1a with $h_{UC}=10$ km than for V1 with $h_{UC}=20$ km, which is also predicted for an upwelling model UPW2 as shown in Fig. 8c–h.

Predicted stratigraphic architectures at 30 Myr for an upwelling model for UPW2 are illustrated in Fig. 8c–h. The width of upwellings is 100 km and the time interval for each upwelling is 3 Myr. The spatial intervals of each upwelling in Fig. 8c–d, e–f and g–h are 50 km, 100 km and 150 km, respectively. The black lines indicate the depositional age at every 3 Myr. The surface of sedimentary basin for each upwelling event is eroded during the uplift phase, and consequently unconformities related to each upwelling are clearly recorded in the sediment architecture. On the other hand, the spatial interval of each upwelling affects the thickness of sedimentary layer, resulting in a thinner sedimentary basin for upwelling model with a larger spatial interval.

Up to now, we have examined the stratigraphic architecture associated with the convective coupling between the uppermost mantle and ductile lower crust. However, stratigraphic evidences for variations in sea-level due to the melting of the polar ice caps, with amplitude of ~100 m and period of ~1 Myr, i.e. third order eustasy (e.g. Vail et al., 1991; Tokuhashi, 1995), have been recorded in observed sediment architectures. Here we examine the effects of third-order eustasy on stratigraphic architecture at areas far away from the polar ice caps. If the eustatic marine regression rate is larger than the tectonic subsidence rate, unconformities reflecting the eustatic events could be formed. Thus, the unconformities provide a sensitive record of both the eustatic events and tectonic movements.

We adopt a viscosity model of V1, an erosion factor (ε) with 0.5 and three eustasy models shown in Fig. 9. The internal load grows up by 1 Myr and keeps its strength after reaching the steady state. The onset time of regression for eustatic models are assumed to be 5 Myr. As the period of the transgression is not important on the formation of unconformity in a simplified model adopted here, the period of transgression is assumed to be the same as that for regression. We define 'regression rate' for a eustatic event as a eustatic sea-level change for regression divided by the period of regression. Fig. 9 depicts the time-dependent changes of the basement at the center of basin. In a eustatic model of EU1, the eustatic sea-level change for regression is 100 m and its period is 0.5 Myr, i.e. regression rate of 0.2 mm yr^{-1}. This eustatic event causes the uplift of ~150 m of the basement, in which we, of course, took into account the effects of erosion associated with the crustal uplift. A eustatic event of EU2, with a regression rate of 0.1 mm yr^{-1}, causes the uplift of ~50 m at most. In an event for EU3, with a regression rate of 0.033 mm yr^{-1}, the uplift

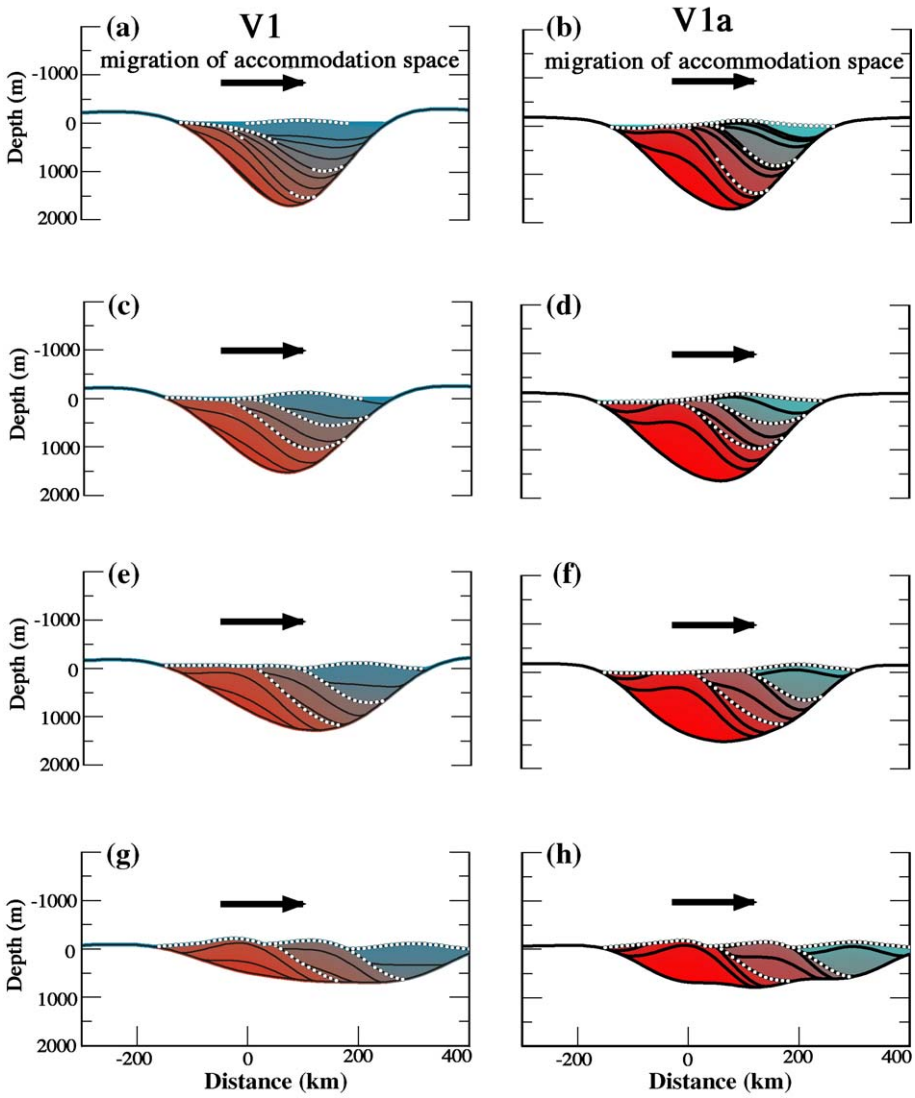

Fig. 8. (a, b) The stratigraphic architecture of sedimentary basin at 20 Myr for continuous model UPW1 in Fig. 7a. The horizontal interval of each upwelling is 50 km. The stratigraphic architectures of sedimentary basin at 30 Myr (c–h) for discontinuous model UPW2 in Fig. 7b. The horizontal interval of each upwelling is 50 km, 100 km, 200 km for (c)–(d), (e)–(f) and (g)–(h), respectively. Model results for (a), (c), (e) and (g) are based on viscosity model V1 and those of (b), (d), (f) and (h) for V1a. We adopt an erosion rate, ε, of 0.5 in these calculations.

is negligibly small. Although we have to take into account the accommodation (depth of sea) in applying these results to actual geological events, our results suggest that the eustatic events, with regression rates less than 0.1 mm yr^{-1} such as those for EU2 and EU3, may not be recorded as unconformity in observed stratigraphic architecture.

The above results for the formation of unconformity are sensitive to the rate of tectonic subsidence. As the subsidence rate due to convective coupling becomes slower with time, unconformities associated with eustatic events may be easily formed in the later stage of the formation of sedimentary basin. In our simplified models, therefore, the unconformity is recorded when the regression rate for the marine regression is larger than the rate of tectonic subsidence. Of course, the unconformity formed in the uplift phase is eroded immediately and not recorded in stratigraphic architecture (see Fig. 6b and c).

4. Discussion

Before discussing the geological application to Karatsu-Sasebo coalfield, we should point out several

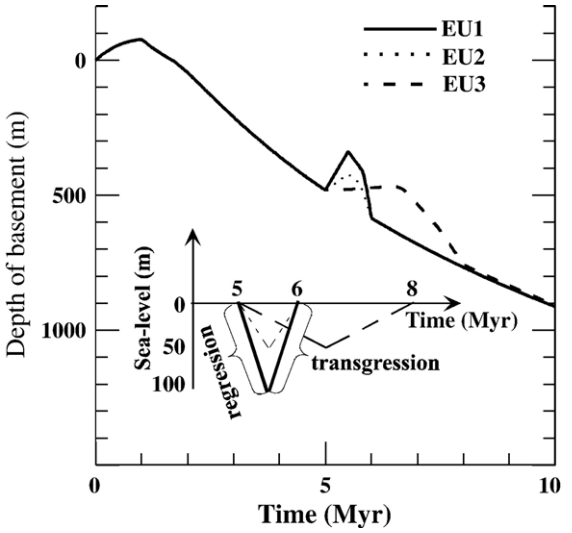

Fig. 9. Time-dependent changes of basement depth. Three eustasy models (EU1, EU2 and EU3) are adopted to examine the effects of eustatic sea-level change on the stratigraphic architectures. Each eustatic event is composed of regression and transgression stages, and characterized by a period and amplitude of sea-level change.

differences between our simple model and recent numerical models. The most crucial differences are probably treatments for (i) rheological structure of the lithosphere and (ii) surface processes such as sedimentation and erosion and an interaction between surface and subsurface processes. Two types of rifting, leading to the formation of sedimentary basin, have been postulated; denoted active and passive, depending on the driving force (e.g. McKenzie, 1978; Sengor and Burke, 1978; Morgan and Baker, 1983; Turcotte and Emerman, 1983; Cloetingh and Kooi, 1992). Recent studies for this topic (e.g. Burov and Cloetingh, 1997; Burov and Poliakov, 2001; Huismans et al., 2001) have generally employed a nonlinear brittle–elastic–ductile rheology based on rock mechanics data (e.g. Goetze and Evans, 1979; Ranalli, 1995; Kohlstedt et al., 1995). Nonlinear rheology is certainly an important factor for determining time and spatial scales and stress concentration, particularly for focused deformation leading to rifting and/or seafloor spreading. Also, nonlinear rheology for the lithosphere will be required in investigating what controls the symmetric or asymmetric extension mode discussed by Huismans et al. (2005), because the stress concentration associated with focused deformation plays an essential role on this problem. The sedimentary basin examined here, however, is formed without focused deformation, and the present model may be applied to the modelling of prerift phase for an earth model with no lithospheric lid.

It should also be noted that Huismans et al. (2001) indicated the transition from passive to active rifting by incorporating the gravitational instability of the lithosphere. They indicated that the thermal buoyancy related to the asthenospheric doming, initially caused by passive rifting, drives active upwelling in a lithosphere scale convection cell. This model may explain the differential stretching with greater extension in the mantle lithosphere than in the crust observed in many rifted basins (e.g. Royden and Keen, 1980). The convective coupling model examined here may be similar to the model by Huismans et al. (2001) in that the convective flow of the uppermost mantle is directly coupling to the ductile lower crustal flow.

Surface processes such as sedimentation and erosion provide important effects on the lithospheric deformation and also on the mechanical structure of the lithosphere. Burov and Cloetingh (1997) and Burov and Poliakov (2001), for example, extensively investigated the surface processes and an interaction between the surface and subsurface processes. They employed a nonlinear rheology and plausible physical models for sedimentation and erosion described by diffusion equation. Then, they numerically indicated that the surface processes change the thermomechanical structure and the subsurface processes through the temperature changes due to the sedimentation and erosion. These processes may have provided important effects on the formation of coalfield in some evolutionary phase of the formation of sedimentary basin. By keeping these points and the limitations of our model in mind, we discuss whether we can extract information about eustatic events and mantle diapiric upwelling from observed stratigraphic architecture.

A sequence stratigraphy has a concept that the sediment body with a distinctive structure is formed by the process associated with the relative sea-level change (Haq et al., 1987). One depositional sequence is defined as a unit bounded by unconformities (e.g. Homewood et al., 1999). The unconformities are formed when the depositional sediment is exposed and/or eroded in the lowering stage of relative sea level followed by sedimentation in the transgressive stage, resulting in sequence stratigraphy. Considering the concept of sequence stratigraphy, our results of the stratigraphic architecture shown in Fig. 8c–d, e–f and g–h may correspond to ‘aggradation+progradation’, ‘progradation’ and ‘downward shift’, respectively (Homewood et al., 1999). In our simplified model, of course, we cannot discuss the source area of sediments for the sedimentary basin and the role of fault movements on the formation

of unconformities. However, it may be possible to draw some information about mantle diapiric upwelling from large-scale sequence stratigraphy.

Finally we apply our model to Karatsu-Sasebo coalfield. Karatsu-Sasebo coalfield located in the northwestern Kyushu (Fig. 10a) is a sedimentary basin formed in the Tertiary. The sedimentary basin, with a width of ~70 km, becomes younger from the southeast to northwest (Aihara et al., 1987). Four main depositional sequence groups have been geologically described (Iwata and Kameo, 2001) (see Fig. 10a), and the thickness of the sedimentary basin is deeper toward the northwest direction, from ~1000 m to ~1500 m. The center of sedimentary basin moves from the southeastern part to the northwestern part, with the tilt of the basement toward the northwest. Fig. 10b shows a simplified description for the sedimentary basin compiled by Nakada et al. (1997). The dashed lines indicate unconformities bounding each depositional sequence. We assume that this sedimentary basin was formed continuously in time domain (see Fig. 7a) because the time intervals between the unconformities are short, i.e.

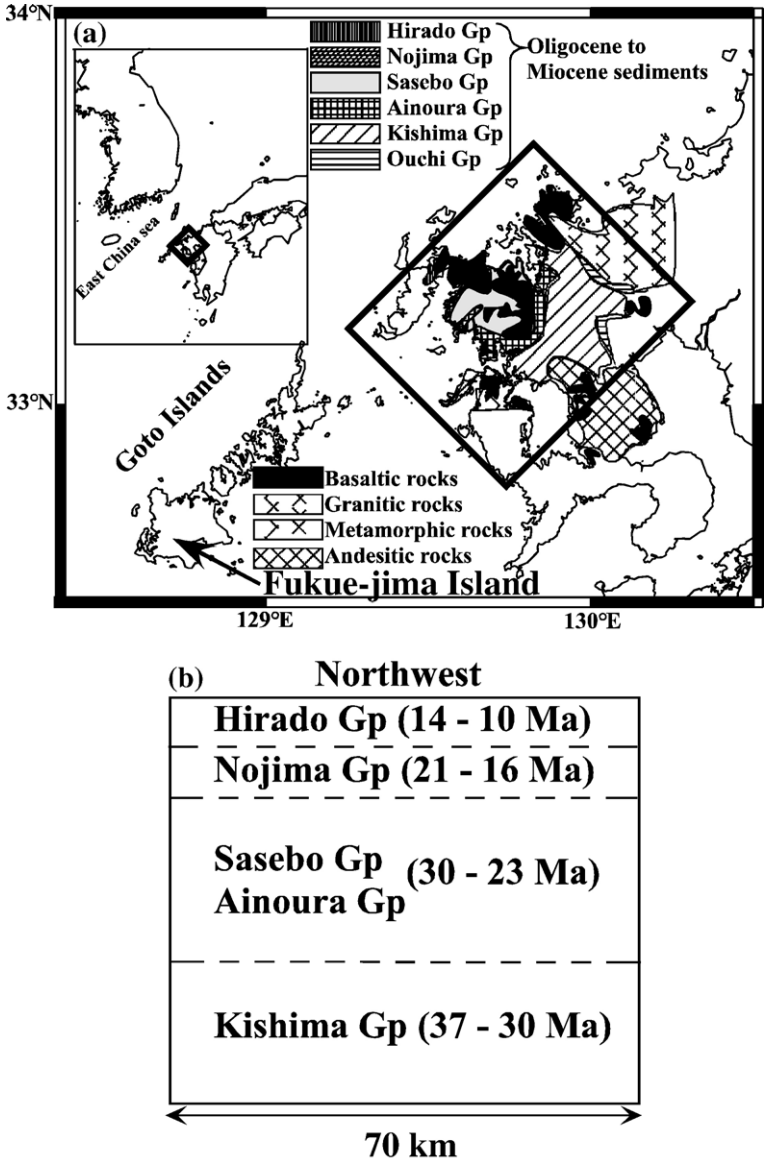

Fig. 10. (a) Geological map of northwestern Kyushu based on compilations by Nakada et al. (1997). The area enclosed by square corresponds to Karatsu-Sasebo coalfield. (b) A simplified description of geological map of Karatsu-Sasebo coalfield. Dashed lines indicate unconformities, and the sediment bodies bounded by unconformities correspond to depositional sequences.

less than 2 Myr. This coalfield was formed by 11 Ma followed by the uplift of ~300 m (max 450 m) and eruption of basalt (Nakada et al., 1997; Yanagi and Maeda, 1998).

We assume the following evolutionary scenario for the sedimentary basin. The mantle diapiric upwelling formed the southeastern part of the coalfield. Then, the northwest migration of the center of sedimentary basin was caused by the northwest migration of upwelling. In this study, we assume that the subsided area is perfectly filled with the sediment, whereas more realistic models have been incorporated in the modeling studies (e.g. Burov and Cloetingh, 1997; Burov and Poliakov, 2001). However, this assumption may be supported from the observations that the depositional conditions were shallow water and non-marine. The ages of small-scale unconformities recorded in the depositional sequences (see Fig. 10b) cannot be explained by the convective coupling alone, and appear to reflect the effects of eustatic fluctuations (Haq et al., 1987) overprinted on the crustal movements. The eustatic event at ~30 Ma in Fig. 11a has been recognized in several areas such as U.S. Middle Atlantic continental margin and Irish continental margin (e.g. Miller et al., 1985), and therefore appears to be a global event. Here all third order eustatic events compiled by Haq et al. (1987) are assumed to be global events. Fig. 11a shows the eustatic curve during the formation period of Karatsu-Sasebo coalfield, and Fig. 11b shows a simplified eustatic model incorporated into our model. By adopting the simplified eustatic model, we examine the effects of regression rate on the formation of unconformity.

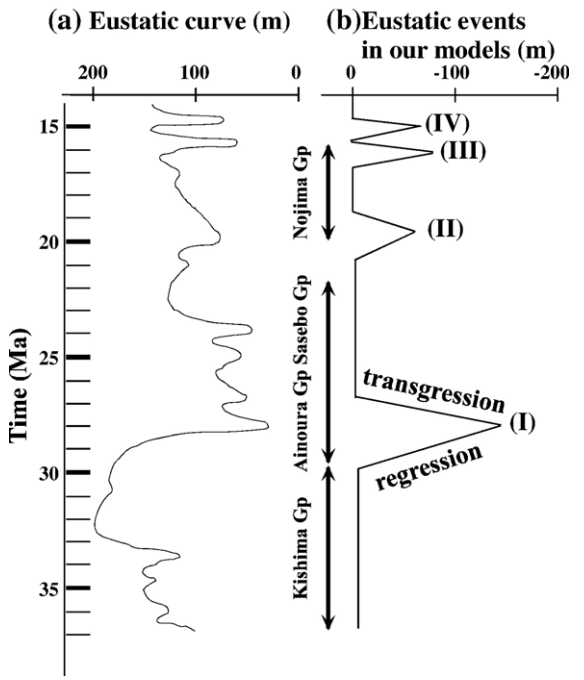

Fig. 11. (a) Eustatic curve by Haq et al. (1987); (b) simplified eustatic model adopted for prediction of Fig. 12.

The stratigraphic architecture of Fig. 12 was simulated by incorporating the effects of eustatic events (I~IV) (Fig. 11b) into the convective coupling model. The mantle diapiric upwelling grows up by 1 Myr and keeps its strength until 5 Myr, followed by migration with 0.5 cm yr^{-1} in the horizontal direction. At 35 Myr, the upwelling starts decaying with a decay period of 5 Myr. The viscosity model is V1, and the erosion rate is 0.5. The viscosity model V1 has no lithospheric lid. This may be supported from the temperature estimates around the Moho (Umino and Yoshizawa, 1996; Nakada et al., 1997) and several geophysical studies based on Holocene sea-level changes (Nakada et al., 1998), seismic tomography (Sadeghi et al., 2000) and electrical conductivity (Shimoizumi et al., 1997). In fact, Nakada et al. (1998) estimated the viscosity of uppermost mantle to be $(1–10)\times10^{19}$ Pa s from Holocene sea-level changes. Also, the ductile lower crust has been suggested by rock mechanics data and the temperature field (Tatsumi et al., 1983; Shimamoto, 1993; Umino and Yoshizawa, 1996; Nakada et al., 1997), and indirectly inferred from the seismicity in the crust (Uehira et al., 2001). However, it is difficult to estimate the viscosity itself.

Fig. 12 illustrates the simulated stratigraphic architecture at 40 Myr after an onset of mantle diapiric upwelling, corresponding to the present in our scenario. The black lines indicate the depositional age at every 4 Myr and the open circles indicate unconformities. The accommodation space migrates toward migrating direction of the upwelling, and the thickness is deeper toward the migrating direction. This result is consistent with the observation that the total thickness of the Tertiary sediment is thicker in the southwestern part of the sedimentary basin. The migration of accommodation space causes the tilt of the basement, and the predicted gradient is about 0.8°. Fig. 13 shows the time-dependent change of the basement depth at $x=0$ km in Fig. 12 (shown as asterisk), corresponding to the uplifted area inferred from geological observations (Yanagi and Maeda, 1998). This result indicates the basement uplift of ~150 m during the past 10 Myr, rather consistent with the observed uplift of ~300 m for Karatsu-Sasebo

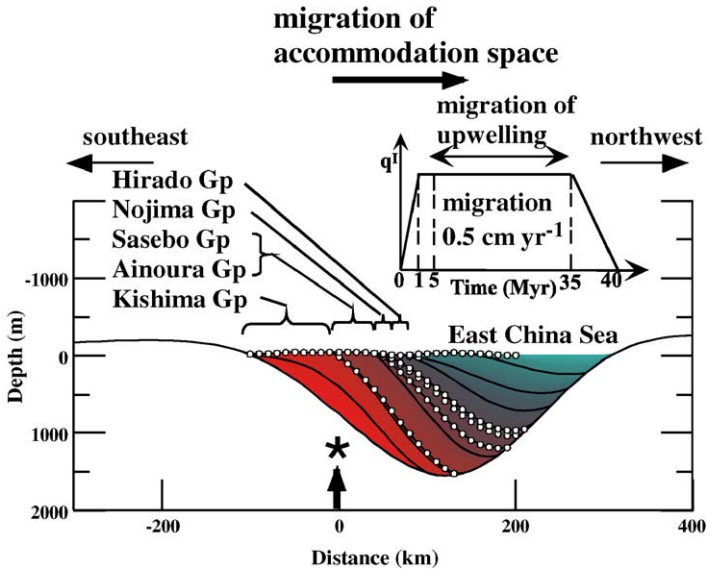

Fig. 12. Simulated stratigraphic architecture at 40 Myr for a eustatic model shown in Fig. 11b, corresponding to Karatsu-Sasebo coalfield. Upwelling model in time domain is also shown. We adopt viscosity model V1 and erosion rate, ε, of 0.5.

coalfield after formation of the sedimentary basin. On the other hand, Nakada et al. (1997) qualitatively suggested that the melt due to adiabatic mantle diapiric upwelling accumulates beneath the lower crust and the accumulation consequently weakens the mechanical coupling. Then, the lower crust recovers its original thickness, and accumulation of low-density melt causes crustal uplift observed in the eastern part of the sedimentary basin. Whereas it is difficult to quantitatively evaluate the responses involving the effects of accumulation of low density melt, we can state at least that the present model quantitatively explains this observation.

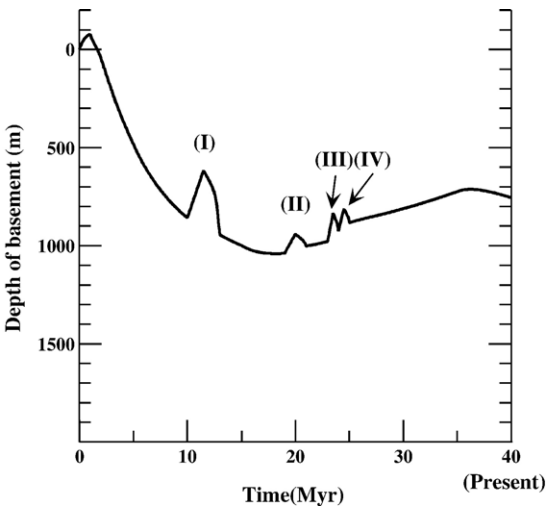

Fig. 13. Time-dependent changes of basement depth at 0 km of Fig. 12 (at the position indicated by asterisk). The numbers of (I), (II), (III) and (IV) shown in this figure correspond to the eustatic events of Fig. 11b.

In Fig. 12, we also indicate the correspondence between observed and predicted sedimentary units bounded by unconformities. Although the horizontal scale is different form the observation, it seems to be consistent with observations that the sedimentary layers become younger from southeast to northwest. Of course, it is difficult to compare the predicted horizontal scale with observed one because we do not have observations about the configuration of original basement. It may be possible to interpret the geological evidences as follows. The eustatic event I occurred at 30 Ma, with amplitude of 150 m and period of 3 Myr (regression rate of 0.1 mm yr^{-1}) (see Fig. 11b), led to the formation of unconformity between Kishima Group and Ainoura Group. The eustatic event II at 21 Ma, with the amplitude of 50 m and the period of 2 Myr (regression rate of 0.05 mm yr^{-1}), is related to the unconformity between Sasebo Group and Nojima Group. Eustatic sea-level changes for events III and IV, with period of 1 Myr, are 80 m and 60 m, respectively. The regression rate is 0.16 mm yr^{-1} for the event III, and 0.12 mm yr^{-1} for the event IV. Eustatic events III and IV at 17 and 16 Ma formed unconformities in proximity to each other, corresponding to those for Nojima Group and Hirado Group. Other small-scale regressions in Fig. 11a, with smaller

regression rates compared with the tectonic subsidence rate, cannot lead to the formation of unconformity in our model. Of course, if the tectonic subsidence rate caused by the convective coupling is slower than the regression rate, then geological evidences associated with the eustatic sea-level changes are recorded as unconformities, and vice versa for faster tectonic subsidence rate.

5. Conclusions

In this study, we examined the stratigraphic architecture of sedimentary basin induced by mantle diapiric upwelling and eustatic event. The conclusions are as follows.

(1) It is possible to simulate the stratigraphic architecture of sedimentary basin by taking into account the convective coupling between the ductile lower crust and uppermost mantle through mantle diapiric upwelling and third order eustatic sea-level change.
(2) An earth model with viscosities of $\sim 10^{19}$ Pa s for the lower crust and $\sim(1–10)\times 10^{19}$ Pa s for the uppermost mantle is required to form the sedimentary basin with a thickness of ~1500 m within 30 Myr after an onset of mantle diapiric upwelling. The stratigraphic architecture and the total thickness of sedimentary basin are also sensitive to the growth and decay periods and horizontal migration of the activity of upwelling, erosion rate and eustatic sea-level change. In particular, the formation of the unconformity is very sensitive to the tectonic subsidence rate and regression rate of eustatic events (see Fig. 9).
(3) To explain the Tertiary sedimentary basin in the northwest Kyushu by convective coupling model adopted here, we need the horizontal migration of the activity of upwelling with ~0.5 cm yr^{-1} and an earth model with viscosities of $\sim 10^{19}$ Pa s for the lower crust and $\sim(1–10)\times 10^{19}$ Pa s for the uppermost mantle. In this case, the maximum thickness of the sedimentary basin is ~1500 m and the maximum tilt of unconformity is 0.8°. Moreover, eustatic sea-level events with a regression rate greater than ~0.05 mm yr^{-1} are recorded as unconformities in the sedimentary basin if we adopt rheological and upwelling models examined here. The convective coupling model including the effects of eustatic events may explain the observed stratigraphic architecture in the northwest Kyushu, Japan.

Acknowledgments

We thank H. Sano, T. Yanagi and T. Sakai for their valuable comments and discussion. Very constructive comments from M. Sandiford and two anonymous reviewers were helpful in improving the paper. This work was partly supported by the Japan Society for the Promotion of Science (JSPS) (Grand-in-Aid for Scientific Research No. 17340132, 17654088).

References

Aihara, A., Tateishi, M., Maeda, J., Koga, Y., Yoshimura, T., Kasayama, H., Aizawa, J., Tsuruta, K., Yamada, T., Mori, A., 1987. Diagenetic and burial thermal alterations of the Tertiary system analyzed by coalification study in North Kyushu, Japan. Sci. Rep. Kyushu Univ. 15, 103–118.

Burov, E., Cloetingh, S., 1997. Erosion and rift dynamics: new thermomechanical aspects of post-rift evolution of extensional basins. Earth Planet. Sci. Lett. 150, 7–26.

Burov, E., Poliakov, A., 2001. Erosion and rheology controls on synrift and postrift evolution: verifying old and new ideas using a fully coupled numerical model. J. Geophys. Res. 106, 16461–16481.

Byerlee, J.D., 1978. Friction of rocks. Pure Appl. Geophys. 116, 615–626.

Cathles, L.M., 1975. The Viscosity of the Earth's Mantle. Princeton University Press, Princeton, NJ.

Cloetingh, S., Burov, E.B., 1996. Thermomechanical structure of European continental lithosphere: constraints from rheological profiles and EET estimates. Geophys. J. Int. 124, 695–723.

Cloetingh, S., Kooi, H., 1992. Intraplate stresses and dynamical aspects of rifted basins. Tectonophysics 215, 167–185.

Cloetingh, S., Wortel, R., 1986. Stress in the Indo-Australian plate. Tectonophysics 132, 49–67.

Dziewonski, A.M., Anderson, D.L., 1981. Preliminary reference Earth model. Phys. Earth Planet. Inter. 25, 297–356.

Ebinger, C.J., Bechtel, T.D., Forsyth, D.W., Bowin, C.O., 1989. Effective elastic plate thickness beneath East Africa and Afar Plateaus and dynamic compensation of the uplifts. J. Geophys. Res. 94, 2883–2901.

Ehara, S., 1984. Terrestrial heat flow determinations in central Kyushu, Japan. Bull. Volcanol. Soc. Jpn. 29, 75–94 (in Japanese with English abstract).

Fukumitsu, S., Miyamachi, H., Kakuta, T., Goto, K., Umakoshi, K., Shimizu, H., 1997. Pn velocity in Kyushu deduced from travel time analysis local earthquakes. J. Seismol. Soc. Jpn. 50, 353–356.

Goetze, C., Evans, B., 1979. Stress and temperature in the bending lithosphere as constrained by experimental rock mechanics. Geophys. J. R. Astron. Soc. 59, 463–478.

Haq, B.U., Hardenbol, J., Vail, R., 1987. Chronology of fluctuating sea levels since Triassic. Science 235, 1156–1167.

Homewood, P.W., Mauriaud, P., Lafont, F., 1999. Best practices in sequence stratigraphy for explorationists and reservoir engineers. Bull. Cent. Rech. Elf Explor. Prod., Mem. 25 (81 pp.).

Huismans, R.S., Podladchikov, Yu.Yu., Cloetingh, S., 2001. Transition from passive to active rifting: relative importance of asthenospheric doming and passive extension of lithosphere. J. Geophys. Res. 106, 11271–11291.

Huismans, R.S., Buiter, S.J.H., Beaumont, C., 2005. Effect of plastic–viscous layering and strain softening on mode selection during

lithospheric extension. J. Geophys. Res. 110 (B02), 406. doi:10.1029/2004JB003114.
Ishibashi, K., 1970. Petrochemical study of basic and ultrabasic inclusions in basaltic rocks from northern Kyushu, Japan. Mem. Fac. Sci. Kyushu Univ. D 20, 85–146.
Iwata, T., Kameo, K., 2001. Sequence stratigraphy and sedimentary process of coal-bearing sedimentary basins in northwest Kyushu. J. Jpn. Assoc. Pet. Technol. 66 (3), 278–291 (in Japanese with English abstract).
Kaufman, P.S., Royden, L.H., 1994. Lower crustal flow in an extensional setting: constraints from Halloran Hills region, eastern Mojave Desert. J. Geophys. Res. 99, 15723–15739.
Kaus, B.J.P., Connolly, J.A.D., Podladchikov, Y.Y., Schmalholz, S.M., 2005. Effect of mineral phase transitions on sedimentary basin subsidence and uplift. Earth Planet. Sci. Lett. 233, 213–228.
King, S., Anderson, D.L., 1995. An alternative mechanism of voluminous basalt formation. Earth Planet. Sci. Lett. 136, 269–279.
Kohlstedt, D.L., Evans, B., Mackwell, S.J., 1995. Strength of the lithosphere: constraints imposed by laboratory experiments. J. Geophys. Res. 100, 17587–17602.
McKenzie, D., 1978. Some remarks on the development of sedimentary basins. Earth Planet. Sci. Lett. 40, 25–32.
Miller, K.G., Mountain, G.S., Tucholke, B.E., 1985. Oligocene glacio-eustasy and erosion on the margins of the North Atlantic. Geology 13, 10–13.
Morgan, P., Baker, B.H., 1983. Introduction–processes of continental rifting. Tectonophysics 94, 1–10.
Nakada, M., 1994. Convective coupling between ductile lower crust and upper mantle and its tectonic implications. Geophys. J. Int. 118, 579–603.
Nakada, S., 1995. Time and spatial variations of upper mantle beneath northern and central Kyushu, Japan. Earth Mon. 17, 427–429 (in Japanese).
Nakada, S., Kamata, H., 1991. Temporal change in chemistry of magma source under central Kyushu, Southwest Japan: progressive contamination of mantle wedge. Bull. Volcanol. 53, 182–194.
Nakada, M., Lambeck, K., 1989. Late Pleistocene and Holocene sea-level change in the Australian region and mantle rheology. Geophys. J. 96, 497–517.
Nakada, M., Yanagi, T., Maeda, S., 1997. Lower crustal erosion induced by mantle diapiric upwelling: constraints from sedimentary basin formation followed by voluminous basalt volcanism in northwest Kyushu, Japan. Earth Planet. Sci. Lett. 146, 415–429.
Nakada, M., Okuno, J., Yokoyama, Y., Nagaoka, S., Takano, S., Maeda, Y., 1998. Mid-Holocene underwater Jomon sites along the west coast of Kyushu, Japan, hydro-isostasy and asthenospheric viscosity. Quat. Res. (Japan) 37, 315–323.
Petrini, K., Connolly, J.A.D., Podladchikov, Yu.Yu., 2001. A coupled petrological–tectonic model for sedimentary basin evolution: the influence of metamorphic reactions on basin subsidence. Terra Nova 13, 354–359.
Podladchikov, Y.Y., Poliakov, A.N.B., Yuen, D.A., 1994. The effect of lithospheric phase transitions on subsidence of extending continental lithosphere. Earth Planet. Sci. Lett. 124, 95–103.
Ranalli, G., 1995. Rheology of the Earth. Chapman & Hall, London.
Royden, L., Keen, C.E., 1980. Rifting process and thermal evolution of the continental margin of eastern Canada determined from subsidence curves. Earth Planet. Sci. Lett. 51, 343–361.
Sadeghi, H., Suzuki, S., Takenaka, H., 2000. Tomographic low-velocity anomalies in the uppermost mantle around the northeastern edge of Okinawa trough, the back arc of Kyushu. Geophys. Res. Lett. 27, 277–280.
Sato, H., 1994. The relationship between late Cenozoic tectonic events and stress field and basin development in northeast Japan. J. Geophys. Res. 99, 22261–22274.
Schmeling, H., Marquart, G., 1990. A mechanism for crustal thinning without lateral extension. Geophys. Res. Lett. 17, 2417–2420.
Sclater, J.G., Christie, P.A.F., 1980. Continental stretching: an explanation of the post-mid-Cretaceous subsidence of the central North Sea basin. J. Geophys. Res. 85, 3711–3739.
Sengor, A.M.C., Burke, K., 1978. Relative timing of rifting and volcanism on Earth and its tectonic applications. Geophys. Res. Lett. 5, 419–421.
Shimamoto, T., 1993. Rheology of rocks and plate tectonics. In: Brown, E.T. (Ed.), Comprehensive Rock Engineering, vol. 1. Elsevier, pp. 93–109.
Shimoizumi, M., Mogi, T., Nakada, M., Yukutake, T., Handa, S., Tanaka, Y., Utada, H., 1997. Electrical conductivity anomalies beneath the western sea of Kyushu, Japan. Geophys. Res. Lett. 24, 1551–1554.
Tanaka, A., Yamano, M., Yano, Y., Sasada, M., 2004. Geothermal Gradient and Heat Flow Data in and around Japan. Digital Geoscience Map DGM P-5, Geological Survey of Japan, AIST, Tsukuba.
Tatsumi, Y., Sakuyama, M., Fukuyama, H., Kushiro, I., 1983. Generation of arc basalt magmas and thermal structure of the mantle wedge in subduction zones. J. Geophys. Res. 88, 5815–5825.
Tokuhashi, S., 1995. Sea-level change and sedimentation: introduction of sequence stratigraphy. Chishitsu News 487, 26–35 (in Japanese).
Turcotte, D.L., Emerman, S.H., 1983. Mechanisms of active and passive rifting. Tectonophysics 94, 39–50.
Turcotte, D.L., Schubert, G., 1982. Geodynamics: Applications of Continuum Physics to Geological Problems. John Wiley, New York.
Uehira, K., Shimizu, H., Matsuwo, N., Goto, K., 2001. The detailed structure of the deep seismic zone and focal mechanism solutions in and around the Kyushu district, Japan. Earth Mon. 23, 669–673 (in Japanese).
Umino, S., Yoshizawa, E., 1996. Petrology of ultramafic xenoliths from Kishyuku lave, Fukue-jima, Southwest Japan. Contrib. Mineral. Petrol. 124, 154–166.
Uyeda, S., 1972. Heat flow. In: Japanese National Committee for Upper Mantle Project (Ed.), The Crust and upper Mantle of the Japanese Area: Part I. Geophysics, Earthq. Res. Inst. Univ. Tokyo, pp. 97–105.
Vail, P.R., Audemard, F., Bowman, S.A., Eisner, P.N., Perez-Cruz, G., 1991. The stratigraphic signatures of tectonics, eustasy and sedimentation–an overview. In: Einsele, G., Ricken, W., Seilacher, A. (Eds.), Cycles and Events in Stratigraphy. Springer, Berlin, pp. 617–659.
Watts, A.B., 2001. Isostasy and Flexure of the Lithosphere. Cambridge University Press, Cambridge.
Weissel, J.K., Karner, G.D., 1989. Flexural uplift of rift flanks due to mechanical unloading of the lithosphere during extension. J. Geophys. Res. 94, 13919–13950.
Wolf, D., 1985. The normal modes of a layered, incompressible Maxwell half-space. J. Geophys. 57, 106–117.
Wu, P., Peltier, W.R., 1982. Viscous gravitational relaxation. Geophys. J. R. Astron. Soc. 70, 435–485.
Yamasaki, T., Nakada, M., 1997. The effects of the spinel–garnet phase transition on the formation of rifted sedimentary basins. Geophys. J. Int. 130, 681–692.

Yanagi, T., Maeda, S., 1998. Magma evolution observed in the Matsuura basalts in northwest Kyushu, Japan: an example of high-pressure open system fractional crystallization in a refilled magma chamber near the crust–mantle boundary. Phys. Earth Planet. Inter. 107, 203–219.

Yoshii, T., 1972. Features of the upper mantle around Japan as inferred from gravity anomalies. J. Phys. Earth 20, 23–34.

Yoshii, T., 1979. Compilation of geophysical data around the Japanese Islands (I). Bull. Earthq. Res. Inst. 54, 75–117 (in Japanese).

Yoshii, T., Asano, S., 1972. Time-term analyses of explosion seismic data. J. Phys. Earth 20, 47–57.

Zhao, D., Horiuchi, S., Hasegawa, A., 1992. Seismic velocity structure of the crust beneath the Japan Islands. Tectonophysics 12, 289–301.